Electronic Spectra of $M(CO)_6$ (M = Cr, Mo, W) Revisited by a Relativistic TDDFT Approach

Angela Rosa,*,† Evert Jan Baerends,*,‡ Stan J. A. van Gisbergen,‡ Erik van Lenthe,‡ Jeroen A. Groeneveld,‡ and Jaap G. Snijders§

Contribution from the Dipartimento di Chimica, Università della Basilicata, Via N. Sauro, 85, 85100 Potenza, Italy, Afdeling Theoretische Chemie, Vrije Universiteit, De Boelelaan 1083, 1081 HV Amsterdam, The Netherlands, and Theoretical Chemistry, Materials Science Centre, Rijksuniversiteit Groningen, Nijenborgh 4, 9747 AG Groningen, The Netherlands

Received March 8, 1999. Revised Manuscript Received August 30, 1999

Abstract: Relativistic time dependent density functional calculations have been performed on the excited states of the $M(CO)_6$ (M = Cr, Mo, W) series. Our results, in agreement with previous density functional[1] and ab initio[2] calculations on $Cr(CO)_6$, indicate that in all members of the series the lowest excited states in the spectra do not correspond to ligand field (LF) excitations, as has been accepted in the past. Instead they correspond to charge transfer (CT) states. The LF excitations are calculated at much higher energy than suggested by the original assignment by Beach and Gray[3] and at different energy along the $M(CO)_6$ series, being much higher in the heavier carbonyls than in $Cr(CO)_6$. These results lead to a definitive reassessment of the role of the LF states in the photochemical dissociation of the metal−CO bonds in the $M(CO)_6$ series, suggesting that the experimentally observed photodissociation of the M−CO bond upon irradiation into the lowest energy bands occurs in the heavier carbonyls, as it does in $Cr(CO)_6$, from CT and not from LF states. A comparison with the experimental data available and, in the case of $Cr(CO)_6$, also with high-level correlated ab initio calculations[2] proves the reliability of the present TDDFT approach. The choice of the exchange−correlation (XC) functional is found to have a large effect on the excitation energies, demonstrating that even for quite "normal", low-lying excitations the XC functional may play an important role. In the heavier carbonyls, mostly in $W(CO)_6$, relativistic effects are seen to be relevant for the LF states as well as for the CT states arising from the $(2t_{2g})^5(3t_{2g})^1$ configuration.

1. Introduction

The electronic spectra of metal hexacarbonyls, $M(CO)_6$ (M = Cr, Mo, W), are very similar to each other.[4,3] They are dominated by two very intense absorption bands, which can be identified as the only two orbitally and spin allowed $^1A_{1g}\rightarrow{}^1T_{1u}$ metal-to-ligand charge-transfer (CT) excitations. In addition, weak shoulders can be observed at the low-energy side of the first charge-transfer band and a not well resolved shoulder appears between the two intense charge-transfer bands. The low-energy shoulders were assigned by Gray and Beach[4] as vibrational components of the ligand field (LF) excited state $^1T_{1g}$ belonging to the $t_{2g}^5e_g^1$ configuration, while the higher energy shoulders at 4.83, 4.66, and 4.54 eV in $Cr(CO)_6$, $Mo(CO)_6$, and $W(CO)_6$, respectively, were assigned to the $^1T_{2g}$ ($t_{2g}^5eg^1$) LF state. Although the authors themselves were concerned about this assignment because it suggests the LF splitting is the same for chromium, molybdenum, and tungsten carbonyls, it appeared to be confirmed by the original extended-Hückel[4] as well as, in the case of $Cr(CO)_6$, more recent semiempirical INDO/S CI[5] and ab initio RHF [6] calculations. There was also little reason for revision of this assignment, since irradiation in the low-energy shoulder leads to fast ejection of CO, in perfect agreement with the "standard" model of photodissociation being induced by LF excitation.[7,8]

However, our ΔSCF-DFT calculations of the excited states of $Cr(CO)_6$ have recently shown,[1] in contrast to the generally accepted assignment by Gray and Beach[4] but in agreement with the sophisticated CASPT2 calculations by Pierloot et al.,[2] that the low-intensity absorption at the low-energy side of the charge-transfer band is not due to LF excited states, but to symmetry-forbidden CT excitations. [ΔSCF means that separate self-consistent-field calculations are performed to optimize the orbitals of the ground state and the appropriate excited state determinants; CASPT2 refers to multiconfiguration SCF ab initio calculations in which all excitations are taken into account in a certain orbital space (the active space), with second-order perturbation corrections added afterward.] In $Cr(CO)_6$, as in other metal−carbonyl complexes, [9−12] the LF excited states are

† Università della Basilicata.
‡ Vrije Universiteit.
§ Rijksuniversiteit Groningen.

(1) Pollak, C.; Rosa, A.; Baerends, E. J. *J. Am. Chem. Soc.* **1997**, *119*, 7324.
(2) Pierloot, K.; Tsokos, E.; Vanquickenborne, L. G. *J. Phys. Chem.* **1996**, *100*, 16545.
(3) Beach, N. A.; Gray, H. B. *J. Am. Chem. Soc.* **1968**, *90*, 5731.
(4) Gray, H. B.; Beach, N. *J. Am. Chem. Soc.* **1963**, *85*, 2922.
(5) Kotzian, M.; Rösch, N.; Schröder, H.; Zerner, M. C. *J. Am. Chem. Soc.* **1989**, *111*, 7687.
(6) Pierloot, K.; Verhulst, J.; Verbeke, P.; Vanquickenborne, L. G. *Inorg. Chem.* **1989**, *28*, 3059.
(7) Geoffroy, G. L.; Wrighton, M. S. *Organometallic Photochemistry*; Academic: New York, 1979.
(8) Ferraudi, G. J. *Elements of Inorganic Photochemistry*; John Wiley & Sons: New York, 1988.
(9) Rosa, A.; Ricciardi, G.; Baerends, E. J.; Stufkens, D. J. *Inorg. Chem.* **1995**, *34*, 3425.
(10) Rosa, A.; Ricciardi, G.; Baerends, E. J.; Stufkens, D. J. *Inorg. Chem.* **1996**, *35*, 2886.

10.1021/ja990747t CCC: $18.00
Published on Web 10/21/1999

at high energy. This result, already relevant in itself, also led to a reassessment of the role of the LF states in the photochemistry of $Cr(CO)_6$ and other metal−carbonyl complexes. In view of the reassignment of the spectrum of $Cr(CO)_6$ and of the implications for the photochemistry, a theoretical study of the excited states of the molybdenum and tungsten hexacarbonyls is called for. In fact, the electronic spectra of $Mo(CO)_6$ and $W(CO)_6$ have never been theoretically investigated and the assignment by the original extended-Hückel study[4] appears to be quite questionable by now. It is indeed reasonable to believe that the shoulder at the low-energy side of the first charge-transfer band originates in the heavier hexacarbonyls, just as in $Cr(CO)_6$, from CT and not from LF transitions, since the electronic spectra of the $M(CO)_6$ series are very similar and, most importantly, it is unlikely that LF states lie at lower energy in $Mo(CO)_6$ and $W(CO)_6$ than in $Cr(CO)_6$.

The purpose of this paper is to provide a detailed analysis of the spectra of the whole series based upon time dependent density functional theory (TDDFT) calculations. TDDFT provides a first principles method for the calculation of excitation energies within a density functional context. The reliability of the TDDFT approach in obtaining accurate predictions of excitation energies and oscillator strengths is by now well documented.[13−22] It has been successfully used to calculate the excitation energies of higher fullerenes[19]and large organic molecules[18,22,23] as well as, more recently, of transition metal complexes such as Mn_2CO_{10}, $NiCO_4$, and MnO_4^{-}[24] and metalporphyrin.s[25] This work will further support the effectiveness of the approach in the field of transition metal chemistry.

Two approximations are made in the TDDFT excitation energy calculations: one for the usual XC potential v_{XC} and one for the XC kernel f_{XC}, which is the functional derivative of the time-dependent XC potential with respect to the density. The most common and simplest approximation to f_{XC} is the adiabatic local density approximation (ALDA). It should be kept in mind that an adiabatic generalized gradient approximation (AGGA), where the second functional derivative with respect to $\rho(\mathbf{r})$ of the exchange−correlation energy would be used for f_{XC}, is not necessarily an improvement over ALDA. The fact that the GGA XC functional approximates the energy better than LDA does holds no guarantee that its functional derivative would also be more accurate. The approximation used for this XC kernel is not critical, however. It has been established that primarily the quality of the ground-state Kohn−Sham (KS) potential determines the accuracy of the excitation energies.[17,20,21]

It has been found[15−18,26] that the LDA (local density approximation) XC potential gives remarkably good results for transitions to low-lying states. However, a deterioration in the quality of results for higher excitation energies has been noted.[15,18] Casida et al.[21] have recently traced the cause of this deterioration to the incorrect asymptotic behavior of the LDA exchange−correlation potential, which tends to zero much faster than the correct Coulombic $-1/r$ behavior in the outer region of the molecule, a problem from which other popular functionals, such as the gradient corrected functionals (GGA), suffer as well. They have demonstrated that using the asymptotically correct potential of van Leeuwen and Baerends (LB94)[27] in the self-consistent-field step corrects the collapse of the high-lying states observed with LDA or GGA potentials. According to these authors, the states which may be significantly affected by the incorrect asymptotic behavior of the LDA or GGA potentials are the ones which have an LDA or GGA excitation energy higher than $-\epsilon_{HOMO}$ (the negative of the highest occupied molecular orbital energy in the LDA or GGA) and/or involve transitions to unbound virtual orbitals.

More generally, one expects the asymptotic part of the potential to have a considerable effect on diffuse states, which are usually the high-lying ones, but not necessarily the ones which fulfill the above criteria. The choice of the KS potential could therefore be very important for the excited states of the investigated hexacarbonyls, because most of them involve transitions to diffuse virtual molecular orbitals.

To check this specific point and more in general the importance of the choice of the KS potential for the excitation energies of transition metal complexes, the excitation energies of the $M(CO)_6$ series have been computed with two different potentials, the generalized gradient approximated potentials (GGA) by Becke[28] (for exchange) and Perdew[29] (for correlation), BP, and the asymptotically correct Van Leeuwen−Baerends potential,[27] LB94.

In the case of the heavier carbonyls, where relativistic effects need to be taken into account, we use a combined scalar relativistic (SR) ZORA (zero order regular approximation)[30−34] and TDDFT approach.

Before dealing with the spectra of the $M(CO)_6$ series, in section 4, we first discuss in section 3 the ground-state electronic structure of the molecules, with special emphasis on the differences between $Cr(CO)_6$ and the heavier carbonyls. Contrary to the electronic structure of chromium hexacarbonyl that has indeed been the subject of many theoretical studies,[35] the

(11) Rosa, A.; Ricciardi, G.; Baerends, E. J.; Stufkens, D. J. *J. Phys. Chem.* **1996**, *100*, 15346.
(12) Wilms, M. P.; Baerends, E. J.; Rosa, A.; Stufkens, D. J. *Inorg. Chem.* **1997**, *36*, 1541.
(13) Casida, M. Time Dependent Density Functional Response Theory for Molecules. In *Recent Advances in Density Functional Methods*; Chong, D. P., Ed.; World Scientific: Singapore, 1995; Vol. 1, p 155.
(14) Casida, M. E. *Recent Developments and Applications of Modern Density Functional Theory*; Elsevier: Amsterdam, 1996.
(15) Jamorski, C.; Casida, M.; Salahub, D. R. *J. Chem. Phys.* **1996**, *104*, 5134.
(16) Petersilka, M.; Gossmann, U. J.; Gross, E. K. U. *Phys. Rev. Lett.* **1996**, *76*, 1212.
(17) Petersilka, M.; Gross, E. K. U. *Int. J. Quantum Chem. Symp.* **1996**, *30*, 181.
(18) Bauernschmitt, R.; Ahlrichs, R. *Chem. Phys. Lett.* **1996**, *256*, 454.
(19) Bauernschmitt, R.; Ahlrichs, R.; Hennrich, F. H.; Kappes, M. M. *J. Am. Chem. Soc.* **1998**, *120*, 5052.
(20) van Gisbergen, S. J. A.; Koostra, F.; Schipper, P. R. T.; Gritsenko, O. V.; Snijders, J. G.; Baerends, E. J. *Phys. Rev. A* **1998**, *57*, 2556.
(21) Casida, M. E.; Jamorski, C.; Casida, K. C.; Salahub, D. R. *J. Chem. Phys.* **1998**, *108*, 4439.
(22) Stratmann, R. E.; Scuseria, G. E.; Frisch, M. J. *J. Chem. Phys.* **1998**, *109*, 8218.
(23) van Gisbergen, S. J. A.; Rosa, A.; Ricciardi, G.; Baerends, E. J. *J. Chem. Phys.* **1999**, *111*, 2499.
(24) van Gisbergen, S. J. A.; Groeneveld, J. A.; Rosa, A.; Snijders, J. G.; Baerends, E. J. *J. Phys. Chem. A* **1999**, *103*, 6835.
(25) Rosa, A.; Ricciardi, G.; Baerends, E. J.; van Gisbergen, S. J. A. To be submitted for publication.
(26) Bauernschmitt, R.; Häser, M.; Treutler, O.; Ahlrichs, R. *Chem. Phys. Lett.* **1997**, *264*, 573.
(27) van Leeuwen, R.; Baerends, E. J. *Phys. Rev. A* **1994**, *49*, 2421.
(28) Becke, A. *Phys. Rev. A* **1988**, *38*, 3098.
(29) Perdew, J. P. *Phys. Rev. B* **1986**, *33*, 8822 (Erratum for p 8834: *Phys. Rev. B* **1986**, *33*, 7406).
(30) Chang, C.; Pelissier, M.; Durand, P. *Phys. Scr.* **1986**, *34*, 394.
(31) Heully, J.-L.; Lindgren, I.; Lindroth, E.; Lundqvist, S.; Màrtensson-Pendrill, A.-M. *J. Phys. B* **1986**, *19*, 2799.
(32) van Lenthe, E.; Baerends, E. J.; Snijders, J. G. *J. Chem. Phys.* **1993**, *99*, 4597.
(33) van Lenthe, E.; Baerends, E. J.; Snijders, J. G. *J. Chem. Phys.* **1994**, *101*, 9783.
(34) van Lenthe, E.; Ehlers, A. W.; Baerends, E. J. *J. Chem. Phys.* **1999**, *110*, 8543.
(35) Davidson, E. R.; Kunze, K. L.; Machado, F. B. C.; Chakravorty, S. *Acc. Chem. Res.* **1993**, *26*, 628.

electronic structure of the heavier hexacarbonyls has never been investigated.

2. Method and Computational Details

The computational method we use is based on the time-dependent extension of density functional theory.[36,13,37] Within the TDDFT framework, excitation energies and oscillator strengths are obtained from the following eigenvalue equation:[13,15,18]

$$\Omega \mathbf{F}_i = \omega_i^2 \mathbf{F}_i \quad (1)$$

In eq 1, the eigenvalues ω_i are the excitation energies, while the oscillator strengths are obtained from the eigenvectors $\mathbf{F}_i$.[13]

For large molecules, such as the ones we consider in this paper, this equation is solved by an iterative technique based on the Davidson algorithm.[38]

The components of the four-index matrix are given by:

$$\Omega_{ia\sigma,jb\tau} = \delta_{\sigma\tau}\delta_{ij}\delta_{ab}(\epsilon_a - \epsilon_i)^2 + 2\sqrt{(\epsilon_a - \epsilon_i)}K_{ia\sigma,jb\tau}\sqrt{(\epsilon_b - \epsilon_j)} \quad (2)$$

where ϵ_a, ϵ_b and ϵ_i, ϵ_j are the energies of the occupied and virtual Kohn−Sham (KS) orbitals, respectively. The matrix K, the so-called coupling matrix, given by

$$K_{ia\sigma,jb\tau} = \int\int \mathrm{d}\mathbf{r}\, \mathrm{d}\mathbf{r}' \phi_{i\sigma}(\mathbf{r})\phi_{a\tau}(\mathbf{r})\left[\frac{1}{|\mathbf{r} - \mathbf{r}'|} + f_{\mathrm{XC}}{}^{\sigma\tau}(\mathbf{r},\mathbf{r}',\omega)\right]\phi_{j\sigma}(\mathbf{r}')\phi_{b\tau}(\mathbf{r}') \quad (3)$$

consists of a Coulomb part and an XC part. In eq 3 the ϕ_i's are the KS orbitals and f_{XC} is the XC kernel mentioned before.

Two steps are involved in the TDDFT procedure, the SCF step to generate the KS orbitals and orbital energies, and a post-SCF step to solve eq 1. In these two steps different approximate functionals may be used.

In this work we use, as is usually done, the Adiabatic Local Density Approximation (ALDA) for the exchange−correlation kernel (post-SCF step), in which the frequency dependence of the kernel is ignored. There is growing evidence that the neglect of frequency dependence is not a severe source of error for low-lying molecular excitation energies, as improvements in the XC potential have been shown to lead to very satisfactory agreement with experiment, although the frequency dependence in the XC kernel is always ignored.[39,40,20]

For the exchange−correlation potentials which determine the KS orbitals ϕ_i and the orbital energies ϵ_i (SCF step) we employ both the BP and LB94 XC potentials mentioned before.

We will use the same notation as used by Casida et al.,[21] which reflects the fact that it is possible to use different functionals for the SCF and post-SCF steps. Thus BP/ALDA and LB94/ALDA indicate that the BP or LB94 functional, respectively, was used for the XC KS potential, and TDLDA means that the functional derivative of the usual LDA XC potential is used for the kernel in the post-SCF step.

The excitation energies of the heavier carbonyls, $Mo(CO)_6$ and $W(CO)_6$, are calculated by a combined scalar relativistic (SR) ZORA (zero-order regular approximation) and TDLDA approach which implies that the one-electron energies and the Kohn−Sham orbitals to be used in eq 1 are obtained by solving the one-electron (SR) ZORA Kohn−Sham equation.[33,34]

One has the choice to use either "scaled" or "unscaled" ZORA orbital energies.

Although the unscaled orbital energies correspond to the eigenvalues of the (SR) ZORA Hamiltonian, we prefer the scaled orbital energies, as these are known[33] to be more reliable for core orbitals. The choice between scaled and unscaled ZORA orbital energies is a rather academic matter in the present study of low-lying excitation energies, as the scaled or unscaled *valence* orbital energies which play a role in these transitions are almost indistinguishable. It has been tested for a few other systems that the difference in excitation energy is therefore negligible for all excitations, except those involving deep-lying core orbitals.

The calculations include all excited ligand-field states, the full range of both spin-allowed and spin-forbidden metal-to-CO transitions as well as the transitions to the metal $(n + 1)$s orbital (Rydberg states).

Our results are compared to the experimental values and in the case of $Cr(CO)_6$ to previous ΔSCF-DFT[1] and CASPT2[2] results. For $Mo(CO)_6$ and $W(CO)_6$, the relativistic effects on the excitation energies are highlighted by comparing relativistic and nonrelativistic TDDFT results.

All calculations reported in this paper have been performed with the ADF-RESPONSE module[41] which is an extension of the Amsterdam Density Functional (ADF) program system.[42−44] The distinctive features of this program include the use of Slater-type orbitals (STOs), a well-balanced numerical integration scheme,[43] a density fitting procedure for the Coulomb-type integrals using auxiliary basis functions (fit functions),[42] and a fully vectorized and parallelized code in combination with the use of symmetry.[44]

For nonrelativistic calculations we use the standard ADF IV basis set[45] which is an uncontracted triple-ζ STO basis set with one 3d polarization function for the C and O atoms and a triple-ζ *n*d, $(n + 1)$s basis with one $(n + 1)$p function for the metals (Cr, Mo, W). The cores (C, O: 1s; Cr: 1s−2p; Mo: 1s−3d; W: 1s−4d) were kept frozen.

For the (SR) ZORA calculations we use an optimized valence basis set that is of the same size as the ADF IV basis described above.[45] The cores (C, O: 1s; Cr: 1s−2p; Mo: 1s−3d; W: 1s−4d) are still kept frozen and described by optimized (SR) ZORA orbitals.

The calculations were performed for both the nonrelativistic and (SR) ZORA optimized O_h geometries of the complexes of the $M(CO)_6$ series. The (SR) ZORA geometries were obtained using the recent implementation of analytical gradients for ZORA in ADF.[34]

In the geometry optimizations the usual (nonrelativistic) BP density functional was used.

3. Ground State Molecular and Electronic Structure of $M(CO)_6$

Geometries and FBDE's of $M(CO)_6$. To assess the accuracy of the relativistic approach used, (SR) ZORA results of geometry optimization and first bond dissociation energies are presented in this section for the three members of the series and compared to the results obtained from other relativistic approaches as well as to results from nonrelativistic GGA-DFT calculations.

Theoretical (nonrelativistic and relativistic) and experimental molecular structures of the hexacarbonyls of chromium, molybdenum, and tungsten are given in Table 1. There we also report, for comparison, ab initio MP2 results by Ehlers et al.[46] as well as results from other DFT relativistic approaches in which the same density functional as in the present work has been used: the quasirelativistic (DFT QR) results by Li et al.,[47] the Douglas−Kroll−Hess DFT results by Nasluzov et al.,[48] the

(36) Gross, E. U. K. *Topics in Current Chemistry*; TDDFT. In Density Functional Theory, Springer Series; Nalewajski, R. F., Ed.; Springer: Heidelberg, 1996.
(37) van Gisbergen, S. J. A.; Snijders, J. G.; Baerends, E. J. *Comput. Phys. Commun.* **1999**, *118*, 119.
(38) Davidson, E. R. *J. Comput. Phys.* **1975**, *17*, 87.
(39) Petersilka, M.; Gossmann, U. J.; Gross, E. K. U. *Electronic Density Functional Theory: Recent Progress and New Directions*; Plenum: New York, 1998.
(40) Tozer, D. J.; Handy, N. C. *J. Chem. Phys.* **1998**, *109*, 10180.
(41) RESPONSE "extension of the ADF program for linear and nonlinear response calculations by van Gisbergen, S. J. A., Snijders, J. G., Baerends, E. J., with contributions by Groeneveld, J. A., Koostra, F., Osinga, V. P.".
(42) Baerends, E. J.; Ellis, D. E.; Ros, P. *Chem. Phys.* **1973**, *2*, 41.
(43) te Velde, G.; Baerends, E. J. *J. Comput. Phys.* **1992**, *99*, 84.
(44) Fonseca Guerra, C.; Visser, O.; Snijders, J. G.; te Velde, G.; Baerends, E. J. Parallelisation of the Amsterdam Density Functional Program. In *Methods and Techniques for Computational Chemistry*; Clementi, E., Corongiu, G., Eds.; STEF: Cagliari, 1995; p 305.
(45) ADF "STO basis set database available on line at http://tc.chem.vu.nl/SCM/Doc/atomicdatabase".
(46) Ehlers, A. W.; Frenking, G. *J. Am. Chem. Soc.* **1994**, *116*, 1514.
(47) Li, J.; Schreckenbach, G.; Ziegler, T. *J. Am. Chem. Soc.* **1995**, *117*, 486.

Table 1. Theoretical and Experimental Bond Lengths (Å) for M(CO)$_6$ (M = Cr, Mo, W)

	Cr(CO)$_6$		Mo(CO)$_6$		W(CO)$_6$	
method	M−C	C−O	M−C	C−O	M−C	C−O
DFT n.r.	1.908	1.156	2.079	1.155	2.106	1.155
(SR) ZORA	1.904	1.156	2.068	1.156	2.062	1.157
DFT QR[a]	1.910	1.153	2.076	1.153	2.049	1.155
DKH DFT[b]			2.068	1.155	2.063	1.157
DFT DPT[c]	1.905	1.159	2.064	1.158	2.060	1.160
MP2[d]	1.861	1.168	2.061	1.164	2.060	1.166
exp[e]	1.918	1.141	2.063	1.145	2.058	1.148

[a] Reference 47. [b] Reference 48. [c] Reference 49. [d] Reference 46; the Cr(CO)$_6$ datum refers to nonrelativistic calculations. [e] Cr(CO)$_6$, ref 51; Mo(CO)$_6$ and W(CO)$_6$, ref 52.

recent results obtained by van Wüllen[49] using the leading order of the relativistic direct perturbation theory (DPT).[50] As inferred from the values reported in Table 1, the (SR) ZORA metal−carbon bond lengths are in excellent agreement with the experimental data,[51,52] especially for the heavier carbonyls where relativistic effects are important. The agreement between (SR) ZORA and other DFT relativistic results, particularly the DFT DPT ones, is also good. The agreement with the MP2 results is good for molybdenum and tungsten. For first-row TM carbonyls, the MP2 method is known to be less successful, [53] so it is not surprising that the MP2 Cr−C bond length is rather too short compared to experiment and the DFT calculations. The relativistic effect on the metal−carbon bond lengths is apparent when comparing DFT nonrelativistic (n.r.) and (SR) ZORA values of Table 1. The bond contraction, as found in the present calculations, is almost negligible for chromium hexacarbonyl (0.004 Å) and increases to 0.011 Å for molybdenum and to 0.044 Å for tungsten, resulting in a maximum for the Mo−CO bond length in agreement with experiment. Without the relativistic bond contraction, the M−CO bond length would increase monotonically down the series.

As for the C−O bond lengths, they show little variation among the members of the series and there is only a small relativistic effect, if any. It is in fact indirect, making the C−O bond longer due to enhanced π-back-donation as the M−C bond shortens due to relativity. The discrepancy between the experimental and theoretical C−O bond lengths as found in the present relativistic and nonrelativistic calculations is not more than 0.015 Å, the theoretical bond lengths being too large. Other DFT relativistic approaches give similar results, while the MP2 C−O bond lengths are even more strongly overestimated compared to experiment.

A further assessment of the accuracy of the (SR) ZORA approach is provided by the first metal−carbonyl bond dissociation energies, FBDEs, computed for the members of the series. These values are reported in Table 3.

An essential step in the determination of FBDE's is the geometry optimization of the pentacarbonyl fragments. The nonrelativistic and (SR) ZORA optimized C_{4v} structures of M(CO)$_5$ (M = Cr, Mo, W) are reported in Table 2. DFT QR[54] and MP2[46] data are also given for comparison. Experimental IR studies reveal that the axial M−CO distance should be shorter than the equatorial M−CO bonds.[55] This is born out by all the theoretical calculations. There is good agreement between (SR) ZORA and MP2 (with relativistic pseudopotentials) distances for M = Mo and W, but DFT QR yields a somewhat larger relativistic M−CO bond contraction for M = W. The Cr−CO distances calculated by the DFT and MP2 schemes differ considerably. It is likely that the MP2 estimates are subject to errors of the same magnitude as in Cr(CO)$_6$. The M−C−O α bond angles optimized at the DFT level are close to 90°, in line with low-temperature matrix IR spectroscopic studies[55] which suggest that this angle in the pentacarbonyls of Cr, Mo, and W is between 90° and 95°, but at variance with MP2 calculations which predict for all members of the M(CO)$_5$ triad α bond angles much smaller than 90°.

Table 2. Calculated Bond Lengths (Å) and Angles (deg) for M(CO)$_5$ (M = Cr, Mo, W)

		DFT n.r.	(SR) ZORA	DFT QR[a]	MP2[b]
Cr(CO)$_5$	r(M−C$_{ax}$)	1.829	1.826	1.848	1.744
	r(M−C$_{eq}$)	1.907	1.903	1.923	1.874
	r(C−O$_{ax}$)	1.164	1.164	1.162	1.192
	r(C−O$_{eq}$)	1.158	1.158	1.154	1.167
	α(C$_{ax}$−M−C$_{eq}$)	90.2	90.2	90.9	86.1
	β(M−C$_{eq}$−O$_{eq}$)	177.3	177.5	179.6	173.7
Mo(CO)$_5$	r(M−C$_{ax}$)	1.956	1.949	1.965	1.930
	r(M−C$_{eq}$)	2.073	2.060	2.083	2.060
	r(C−O$_{ax}$)	1.165	1.166	1.163	1.179
	r(C−O$_{eq}$)	1.157	1.158	1.156	1.165
	α(C$_{ax}$−M−C$_{eq}$)	89.4	89.9	90.2	87.6
	β(M−C$_{eq}$−O$_{eq}$)	177.8	178.4	179.0	175.7
W(CO)$_5$	r(M−C$_{ax}$)	1.978	1.944	1.915	1.944
	r(M−C$_{eq}$)	2.099	2.052	2.045	2.053
	r(C−O$_{ax}$)	1.165	1.167	1.168	1.178
	r(C−O$_{eq}$)	1.157	1.159	1.157	1.167
	α(C$_{ax}$−M−C$_{eq}$)	89.1	90.4	91.2	88.9
	β(M−C$_{eq}$−O$_{eq}$)	177.4	178.6	179.6	177.0

[a] Reference 54. [b] Reference 46; the Cr(CO)$_5$ datum refers to nonrelativistic calculations.

Table 3. Theoretical and Experimental First Bond Dissociation Energy (kcal/mol) for M(CO)$_6$ (M = Cr, Mo, W)

method	Cr(CO)$_6$	Mo(CO)$_6$	W(CO)$_6$
DFT n.r.	41.6	37.2	37.5
(SR) ZORA	42.0	39.6	45.0
DFT QR[a]	46.2	39.7	43.7
DKH DFT[b]		39.3	46.9
DFT DPT[c]	43.7	39.1	46.1
CCSD(T)//MP2[d]	45.8	40.4	48.0
exp[e]	36.8 ± 2	40.5 ± 2	46.0 ± 2

[a] Reference 47. [b] Reference 48. [c] Reference 49. [d] Reference 46; the Cr(CO)$_6$ datum refers to nonrelativistic calculations. [e] Reference 50.

Using the results for the pentacarbonyl fragments, estimates of FBDE's for M(CO)$_6$ (M = Cr, Mo, W) can be given based on (SR) ZORA calculations. They are compared in Table 3 with experimental data[50] and with estimates based on DFT QR,[47] DFT DKH,[48] DFT DPT,[49] and ab initio CCSD(T)//MP2 calculations.[46] It follows from the table that the agreement between theory and experiment is excellent for Mo and W. The situation is different for Cr(CO)$_6$ where all theoretical values are larger than the best experimental estimate of 36.8 kcal/mol which is based on gas-phase laser pyrolysis.[50] If DFT QR and CCSD(T)//MP2 values deviate from the experimental datum by more than 9 kcal/mol, the DFT n.r. and (SR) ZORA values of 41.6 kcal/mol and 42.0 kcal/mol, respectively, are in much better agreement with the experimental estimate. It should be mentioned that CCSD(T) calculations by Barnes et al.[45] predict a first bond dissociation energy of 38 kcal/mol, very close to the experimental result.

(48) Nasluzov, V. A.; Rösch, N. *Chem. Phys.* **1996**, *210*, 413.
(49) van Wüllen, C. *J. Chem. Phys.* **1996**, *105*, 5485.
(50) van Wüllen, C. *J. Chem. Phys.* **1995**, *103*, 3589.
(51) Jost, A.; Rees, B.; Yelon, W. *Acta Crystallogr.* **1975**, *B 31*, 2649.
(52) Arnesen, S. P.; Schmidling, D. G. *J. Mol. Struct.* **1974**, *22*, 466.
(53) Ehlers, A. W.; Dapprich, S.; Vyboischchikow, S. G.; Frenking, G. *Organometallics* **1996**, *15*, 105.
(54) Li, J.; Schreckenbach, G.; Ziegler, T. *J. Phys. Chem.* **1994**, *98*, 4838.
(55) Perutz, R. N.; Turner, J. J. *J. Am. Chem. Soc.* **1975**, *97*, 8400.

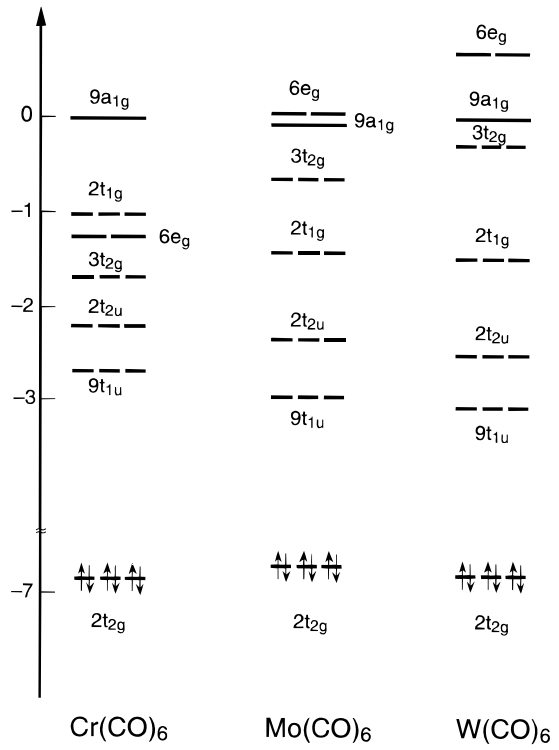

Figure 1. Energy level scheme for $M(CO)_6$ (M = Cr, Mo, W). For the sake of homogeneity with $Cr(CO)_6$, the orbital numbering of $Mo(CO)_6$ and $W(CO)_6$ does not include the 1s−2p cores of Mo, the 1s−2p cores, and the 4f valence orbitals of W.

Relativistic effects are seen to strengthen the M−CO bonds. As inferred from Table 3, for $Cr(CO)_6$, $Mo(CO)_6$, and $W(CO)_6$ the relativistic effects increase the FBDE's by 0.8, 2.4, and 7.5 kcal/mol, respectively, at the (SR) ZORA level.

Electronic Structure of $M(CO)_6$. Before dealing with the excited states of the $M(CO)_6$ series we will briefly discuss the ground-state electronic structure of these molecules, with special emphasis on the salient differences between $Cr(CO)_6$ and the heavier hexacarbonyls, $Mo(CO)_6$ and $W(CO)_6$. The orbital energies, which are a determining factor for the excitation energies, are of particular interest. We therefore show in Figure 1, for the $M(CO)_6$ series, the (nominally) *n*d one-electron levels, the highest occupied orbital $2t_{2g}$, and the empty $6e_g$, as well as the whole set of empty CO $2\pi^*$ and the M−(n + 1)s levels. For $Mo(CO)_6$ and $W(CO)_6$ only the relativistic one-electron levels are shown.

From the level scheme of Figure 1 it may be inferred that the most prominent difference between $Cr(CO)_6$ and the heavier hexacarbonyls is the relative destabilization with respect to the HOMO orbital (of which the energy changes very little along the series) of the M−CO π-antibonding $3t_{2g}$ and even more so of the M−CO σ antibonding $6e_g$. The upward shift of the $3t_{2g}$ and $6e_g$ in going from Cr to Mo and W can be traced primarily to the increase of the M/CO overlap as the diffuseness of M−*n*d orbitals increases in the order 3d < 4d < 5d. We note that the destabilization of the $3t_{2g}$ on going from Cr to W is not mirrored by the stabilization of its bonding counterpart, the $2t_{2g}$. This orbital, which is largely a metal d_π orbital, is very little dependent on the central metal, which is consistent with the experimental ionization potential (IP) data[3] which show the same ionization energy for the $2t_{2g}$ in $Cr(CO)_6$, $Mo(CO)_6$, and $W(CO)_6$. The constant orbital energy (and IP) of $2t_{2g}$, despite the decrease in metal 4d and 5d orbital stability as compared with 3d, was explained by Beach and Gray[3] in terms of an increase of M→CO π-back-donation down the series. The upward shift of the $3t_{2g}$ supports this suggestion.

Comparing relativistic and nonrelativistic orbital energies for the heavier carbonyls, it appears that relativistic effects increase the destabilization of both the $3t_{2g}$ and $6e_g$, mostly in the case of M = W, which can be related to the metal-based d orbitals being destabilized and becoming more diffuse due to relativity. Considering first the σ antibonding $6e_g$ orbital, we note that there are counteracting effects on the position of the $6e_g$, which is mainly (more than 60% d_{z^2}) located on the metal. On one hand there will be destabilization due to relativistic effects and by stronger pushing up by the CO 5σ orbitals due to enhanced overlap/interaction with the more diffuse d_{z^2} orbital. On the other hand relativistic destabilization of the *n*d will lead to an enhanced energy gap with the CO 5σ orbitals, and therefore to less pushing up by the CO 5σ. The net effect is that the $6e_g$ is raised by 0.2 and 0.6 eV in $Mo(CO)_6$ and $W(CO)_6$, respectively. As for the π bonding/antibonding pair of $2t_{2g}/3t_{2g}$ orbitals, the relativistic destabilization of the d_π reduces the $d_\pi-2\pi^*$ gap and thus enhances the metal−CO π-interaction (Li et al.[54] have shown indeed that in $W(CO)_6$ relativistic effects increase the metal to CO π-back-donation). The result is that the $3t_{2g}$ rises by 0.1 and 0.5 eV in Mo and W, respectively, and its bonding counterpart, the $2t_{2g}$, stays put.

The $9a_{1g}$ orbital is rather special. It has mostly metal s character, but it is not simply the M (n + 1)s orbital. Rather, it is very diffuse and actually consists mostly of the next higher s orbital that is obtained in the atomic calculation. This cannot be identified unambiguously with the M (n + 2)s orbital. For one thing, the basis set may not be adequate to describe this very diffuse atomic orbital. Moreover, the BP calculation leads to an asymptotically incorrect Kohn−Sham potential, it goes exponentially to zero and lacks the required $-1/r$ behavior. The higher virtual solutions in the atomic calculation may therefore not be physically meaningful. The (n + 1)s orbital overlaps so strongly with the a_{1g} combination of CO 5σ orbitals that it is very strongly destabilized. Apparently, the nodal structure of the next virtual atomic orbital prevents such large overlap and strong destabilization. The strong participation of this atomic orbital in the $9a_{1g}$ implies very diffuse character of that orbital. The diffuse character of the $9a_{1g}$ orbital may, however, lead to destabilization in condensed phases due to interaction with neigboring molecules. In our calculations on the isolated molecules the position of the $9a_{1g}$ changes very little along the triad, both at the relativistic and the nonrelativistic levels. The orbital is so diffuse that it experiences very little relativistic effects, the relativistic stabilization observed in the tungsten being only 0.01 eV.

Apart from the $3t_{2g}$, which is nominally a $2\pi^*$ orbital but has no less than 40% admixture of metal orbitals, whose behavior along the series has already been discussed, the energy of the remaining empty CO $2\pi^*$ orbitals is very little metal sensitive, although a stabilization of these orbitals occurs on going from $Cr(CO)_6$ to the heavier carbonyls. The central atom (n + 1)p orbitals mix into the $9t_{1u}$, and the stabilization of this orbital along the series is just proportional to the interaction of the metal (n + 1)p orbitals with the t_{1u} combination of the $(CO)_6$ cage which increases in the order 4p < 5p < 6p. As for the $2t_{1g}$ and the $2t_{2u}$ which are antibonding combinations of CO $2\pi^*$ orbitals, their stabilization down the triad is to be related to a relief of the CO−CO antibonding interactions caused by the larger dimension of the $(CO)_6$ cage in the heavier hexacarbonyls compared to $Cr(CO)_6$.

Table 4. Comparison of TDLDA Singlet Excitation Energies (eV) of $Cr(CO)_6$ to Experimental and Theoretical ΔSCF[a] and CASPT2[b] Values[c]

		transition energy (eV)					oscillator strenght		
state	composition	BP/ALDA	LB94/ALDA	ΔSCF[a]	CASPT2[b]	expt[d]	TDDFT BP	CASPT2[b]	expt[d]
a^1E_u	100%($2t_{2g}\rightarrow 9t_{1u}$)	4.01	3.78	4.00	3.41−3.59				
a^1T_{2u}	100%($2t_{2g}\rightarrow 9t_{1u}$)	4.04	3.81	4.00	3.70−3.56				
a^1A_{2u}	98%($2t_{2g}\rightarrow 9t_{1u}$)	4.13	3.89	4.20	3.58−3.58				
a^1T_{1u}	64%($2t_{2g}\rightarrow 9t_{1u}$), 36%($2t_{2g}\rightarrow 2t_{2u}$)	4.19	3.91	5.60	4.54−4.11	4.43	0.03	0.20	0.25
a^1A_{1u}	99%($2t_{2g}\rightarrow 2t_{2u}$)	4.44	4.08	4.50	4.15−4.10				
b^1E_u	100%($2t_{2g}\rightarrow 2t_{2u}$)	4.49	4.13	4.50	3.97−4.05				
b^1T_{2u}	100%($2t_{2g}\rightarrow 2t_{2u}$)	4.50	4.13	5.00	4.32−4.43				
a^1T_{1g}	100%($2t_{2g}\rightarrow 3t_{2g}$)	5.00	4.62	5.69	4.82				
a^1T_{2g}	78%($2t_{2g}\rightarrow 3t_{2g}$), 16%($2t_{2g}\rightarrow 6e_g$)	5.24	4.89	5.33	5.43				
a^1E_g	94%($2t_{2g}\rightarrow 3t_{2g}$)	5.43	5.05	5.75	4.58				
b^1T_{1g}	100%($2t_{2g}\rightarrow 6e_g$)	5.50	5.20	5.66	4.85				
c^1T_{1g}	100%($2t_{2g}\rightarrow 2t_{1g}$)	5.64	5.10	6.23	5.91				
b^1T_{2g}	100%($2t_{2g}\rightarrow 2t_{1g}$)	5.68	5.14	6.25	5.92				
b^1T_{1u}	58%($2t_{2g}\rightarrow 2t_{2u}$), 32%($2t_{2g}\rightarrow 9t_{1u}$)	5.76	5.37	6.50	5.07−5.20	5.41	1.52	2.58	2.30
c^1T_{2g}	79%($2t_{2g}\rightarrow 6e_g$), 11%($2t_{2g}\rightarrow 3t_{2g}$)	5.90	5.61	6.42	5.08				
b^1E_g	80%($2t_{2g}\rightarrow 2t_{1g}$), 7%($8t_{1u}\rightarrow 9t_{1u}$)	6.42	5.89	7.48	5.42				
d^1T_{2g}	100%($2t_{2g}\rightarrow 9a_{1g}$)	6.63	7.47						
b^1A_{1g}	60%($2t_{2g}\rightarrow 3t_{2g}$), 22%($5e_g\rightarrow 6e_g$)	7.55	7.05		6.89				

[a] From ref 1. [b] From ref 2. The energy range indicated for CASPT2 results refers to different choices of active spaces, see ref 2 for details. [c] The one-electron transitions contributing to the TDDFT solution vectors and oscillator strengths are from BP/ALDA calculations. [d] From ref 3.

Orbital energy differences between occupied and virtual KS orbitals can be used as a first-order estimate of excitation energies (cf. eq 2) and are thus useful for qualitative purposes. The orbital energies of $Cr(CO)_6$, $Mo(CO)_6$, and $W(CO)_6$ do not only suggest that in the heavier carbonyls the LF excited states will not be the lowest excited states in the excitation spectrum, just as found in $Cr(CO)_6$,[1] but also that they will lie at higher energy than in $Cr(CO)_6$. The energies of the CT excited states, except for the ones arising from the $(2t_{2g})^5(3t_{2g})^1$ configuration, are expected to change very little down the series.

These suggestions have been verified by explicit calculations of the excited states of these molecules, which will be discussed in the next section.

4. Electronic Spectra of M(CO)$_6$ (M = Cr, Mo, W)

Cr(CO)$_6$. In connection with the theoretical study of the M−CO photodissociation mechanism in $Cr(CO)_6$, we have recently calculated[1] the electronic spectrum of this complex using the ΔSCF-type of approach originally suggested by Ziegler et al.[56] In agreement with CASPT2 calculations,[2] which may be considered the most sophisticated ones to date, we came to an interpretation of the experimental spectrum different from any previously published.

In the present work the electronic spectrum of $Cr(CO)_6$ is revisited using the theoretically better founded time-dependent DFT method with the adiabatic local density approximation.

The BP/ALDA and LB94/ALDA excitation energies calculated for the spin-allowed and the spin-forbidden excited states are presented in Tables 4 and 5, respectively, and compared with the available experimental information for the two allowed charge-transfer states and previous CASPT2[2] and Δ*SCF*[1] results. The tables also include the composition of the BP/ALDA solution vectors in terms of the major one-electron transitions (the composition of the LB94/ALDA solution vectors is very similar and is not reported).

Overall, the interpretation of the electronic spectrum of $Cr(CO)_6$ that emerges from the present TDDFT calculations strongly supports the CASPT2[2] and ΔSCF[1] interpretation according to which the lowest excited states in the $Cr(CO)_6$ spectrum do not correspond to ligand field transitions, as suggested by the original and since then generally accepted assignment by Gray and Beach.[3] Instead they correspond to orbitally-forbidden or spin-forbidden charge-transfer states. All theoretical approaches give indeed the a^1E_u, a^1T_{2u}, a^1A_{2u}, and a^1A_{1u}, b^1E_u, b^1T_{2u} sets of symmetry-forbidden, charge-transfer excitations as the lowest excitations. In $Cr(CO)_6$ as in other d^6 metal−carbonyl complexes[9−12] LF states are at high energy.

When looking at the excitation energy values reported in Tables 4 and 5 in more detail, we notice that the agreement of the TDDFT results, particularly of the LB94/ALDA, with respect to CASPT2 is considerably improved over the ΔSCF results for a number of excited states. The improvement of TDDFT over ΔSCF results is especially noteworthy for the two-spin and orbitally-allowed a^1T_{1u} and b^1T_{1u} excited states which at the ΔSCF level are computed at 5.60 and 6.50 eV,

Table 5. TDLDA Triplet Excitation Energies (eV) of $Cr(CO)_6$ with a Comparison Made to the Δ*SCF*[a] and CASPT2[b] Results[c]

		transition energy (eV)			
state	composition	BP/ALDA	LB94/ALDA	ΔSCF[a]	CASPT2[b]
a^3T_{1u}	96%($2t_{2g}\rightarrow 9t_{1u}$), 4%($2t_{2g}\rightarrow 2t_{2u}$)	3.86	3.62	3.83	3.90−3.69
a^3A_{2u}	99%($2t_{2g}\rightarrow 9t_{1u}$)	3.88	3.66	3.98	
a^3T_{2u}	100%($2t_{2g}\rightarrow 9t_{1u}$)	3.94	3.70	3.87	
a^3E_u	100%($2t_{2g}\rightarrow 9t_{1u}$)	3.97	3.74	4.00	
a^3A_{1g}	99%($2t_{2g}\rightarrow 3t_{2\,g}$)	4.08	3.66	3.91	
b^3T_{1u}	96%($2t_{2g}\rightarrow 2t_{2u}$), 4%($2t_{2g}\rightarrow 9t_{1u}$)	4.35	4.00	4.74	4.51−4.51
b^3E_u	98%($2t_{2g}\rightarrow 2t_{2u}$)	4.37	4.01	4.41	
b^3T_{2u}	98%($2t_{2g}\rightarrow 2t_{2u}$)	4.38	4.03	4.82	
a^3A_{1u}	100%($2t_{2g}\rightarrow 2t_{2u}$)	4.44	4.08	4.54	
a^3E_g	100%($2t_{2g}\rightarrow 3t_{2g}$)	4.65	4.25	4.60	
a^3T_{2g}	100%($2t_{2g}\rightarrow 3t_{2g}$)	4.69	4.30	4.89	
a^3T_{1g}	100%($2t_{2g}\rightarrow 3t_{2g}$)	4.99	4.62	5.33	
b^3T_{1g}	100%($2t_{2g}\rightarrow 6e_g$)	5.17	4.83	4.66	4.28
b^3T_{2g}	100% ($2t_{2g}\rightarrow 6e_g$)	5.19	4.86	5.62	4.64
b^3E_g	100%($2t_{2g}\rightarrow 2t_{1g}$)	5.47	4.92	5.64	
c^3T_{2g}	100%($2t_{2g}\rightarrow 2t_{1g}$)	5.59	5.05	6.16	
c^3T_{1g}	100%($2t_{2g}\rightarrow 2t_{1g}$)	5.63	5.10		
d^3T_{2g}	100%($2t_{2g}\rightarrow 9a_{1g}$)	6.60	7.43		

[a] From ref 1. [b] From ref 2. The energy range indicated for CASPT2 results refers to different choices of active spaces, see ref 2 for details. [c] The one-electron transitions contributing to the BP/ALDA solution vectors are also given.

(56) Ziegler, T.; Rauk, A.; Baerends, E. J. *Theor. Chim. Acta* **1977**, *43*, 261.

respectively, i.e., more than 1 eV higher than the experimental band maxima at 4.43 and 5.41 eV, while good agreement with experiment is obtained at the TDDFT level. The associated oscillator strengths are, however, underestimated compared to experiment, especially in the case of the a^1T_{1u}.

We blame the poor ΔSCF results for the a^1T_{1u} and b^1T_{1u} excited states on the inability of this approach to account for the configuration mixing occurring in these states. Looking indeed at the composition of the BP/ALDA solution vectors, we notice that the states under consideration have a multiple transition character, consisting of the same two transitions, the $2t_{2g}\rightarrow 9t_{1u}$ and the $2t_{2g}\rightarrow 2t_{2u}$, with approximately reversed weights. The multiconfigurational character of the a^1T_{1u} and b^1T_{1u} excited states also emerges from CASPT2 calculations. As can be seen in Table 5, ΔSCF results for the corresponding triplets, a^3T_{1u} and b^3T_{1u} which are almost pure states, compare much better with both CASPT2 and TDDFT results.

The TDDFT results for the LF transitions are also on the whole improved compared to ΔSCF. The ΔSCF energies for singlet LF states, b^1T_{1g} and c^1T_{2g}, are h 5.66 and 6.42 eV, respectively, rather high compared to the CASPT2 values of 4.85 and 5.08 eV. For the downshifted LB94/ALDA energies the discrepancy is considerably diminished, the singlet LF states b^1T_{1g} and c^1T_{2g} being calculated at 5.20 and 5.61 eV. For the corresponding triplets b^3T_{1g} and c^3T_{2g} the trends are different. The b^3T_{1g} ΔSCF energy of 4.66 eV is closer to the CASPT2 value 4.28 eV than the TDDFT energies, which are both at the BP/ALDA and the LB94/ALDA levels, upshifted with respect to ΔSCF. For c^3T_{2g} the Δ*SCF* result is, as for the singlets, rather high (5.62 eV compared to 4.64 eV for CASPT2), the LB94/ALDA energy of 4.86 eV being in much better agreement with CASPT2.

Comparing BP/ALDA and LB94/ALDA results it is apparent that the choice of the *xc* functional has a large effect on the excitation energies of both singlet and triplet states, the LB94 results being usually, but not invariably, closer to CASPT2 than the BP ones.

The significant effect of the asymptotic correction embodied in the LB94 potential cannot simply be ascribed to Rydberg character of the excited states. In recent work by Casida et al.[21] it was suggested that the incorrect asymptotic behavior of the LDA or BP potentials will have adverse consequences for excitations that lie close to or above the ionization threshold, $-\epsilon_{HOMO}$, which in this specific case is −6.6 eV. However, none of the considered excited states, apart from the b^1E_g, $d^{1,3}T_{2g}$, and b^1A_{1g}, meets this criterium. It is still possible that the observed energy shift from BP/ALDA to LB94/ALDA, which is never less than 0.2 eV, is related to the diffuse character of most of these excited states, since they involve transitions to pure CO $2\pi^*$ orbitals and hence will be affected by the asymptotic part of the potential. It is, however, worth noting that the LF states, which from the composition of the BP/ALDA solution vectors one can recognize as the $b^{1,3}T_{1g}$ and $c^{1,3}T_{2g}$ states, also show some 0.3 eV shift going from BP to LB94. This is somewhat surprising in view of the fact that these states are largely d−d and therefore located on the metal. They of course also have considerable CO $2\pi^*$ character (in the HOMO $2t_{2g}$) and 5σ character (in the $6e_g$), which might make them sensitive to the asymptotic potential. However, the lowering observed in going from BP/ALDA to LB94/ALDA may not be exclusively due to the improved asymptotic behavior of the LB94 XC potential. In fact, the LB94 potential also changes the usual LDA or GGA XC potentials in the inner region of the molecule, and this also affects the values of the excitation energies. We have observed for the free base porphin molecule[23] that the low-lying LB94/ALDA excitation energies were typically 0.1 eV lower than the BP results, although we considered only low-lying excitation energies there. For the two lowest excitation energies of $Mn_2(CO)_{10}$, LB94 also gives a significant decrease in excitation energy, in that case worsening agreement with experiment.[24]

A transition that warrants special comment is the one to the metal-$9a_{1g}$ orbital. The metal-$9a_{1g}$ orbital is very diffuse, being mostly (90%) the first virtual atomic orbital in the atomic Cr calculation. The diffuse character of the $9a_{1g}$ is also evident from the very small singlet−triplet splitting of the excited states. One expects the very diffuse character of these excited states to make them particularly sensitive to the asymptotic character of the KS potential. The d^1T_{2g} and d^3T_{2g} excited states in fact experience the largest shift in going from BP to LB94, from 6.63 and 6.60 eV at the BP/ALDA level to 7.47 and 7.43 eV at the LB94/ALDA level. It is, however, worth noting that the d^1T_{2g} and d^3T_{2g} excitations are the only ones which are shifted *upward* by the LB94 potential.

Summarizing we note that an overall comparison with experiment (for the allowed a^1T_{1u} and b^1T_{1u} states) and with the CASPT2 results gives a mixed picture. The LB94/ALDA excitation energy is too low for a^1T_{1u} and just right for b^1T_{1u}, while the reverse holds for the CASPT2 excitation energies. For the singlet LF states the LB94 potential, compared to the BP potential, brings the excitation energies down and closer to the CASPT2 results, but the LB94/ALDA excitation energies are still 0.2−0.5 eV higher than CASPT2. The downshift caused by the LB94 potential compared to the BP potential is a general phenomenon (with the one exception of the $d^{1,3}T_{2g}$, see above). The LB94 excitation energies are on the average closer to the CASPT2 results, but they may both be above and below the CASPT2 energies, as was already noted for the experimentally observed a^1T_{1u} and b^1T_{1u} states.

$Mo(CO)_6$ and $W(CO)_6$. The spectra of $Mo(CO)_6$ and $W(CO)_6$ are very similar to the spectrum of $Cr(CO)_6$. They are dominated by two very intense absorption bands, which can be identified as the only two orbitally- and spin-allowed $^1A_{1g}\rightarrow{}^1T_{1u}$ metal-to-ligand charge-transfer excitations. In addition, three weak shoulders can be observed at the low-energy side of the first charge-transfer band, and a (not well resolved) shoulder appears between the two intense charge-transfer bands. The higher energy components of the low-energy shoulders at 3.63, 3.83, and 4.05 eV in $Mo(CO)_6$ and at 3.54, 3.74, and 3.96 eV in $W(CO)_6$ were assigned by Beach and Gray[3] as vibrational components of the ligand field excited state $^1T_{1g}$ belonging to the $t_{2g}^5eg^1$ configuration, while the lowest energy component which is much weaker in $Mo(CO)_6$ than in $W(CO)_6$ and is not seen at all in $Cr(CO)_6$, was assigned as the spin-forbidden $^1A_{1g}\rightarrow{}^3T_{1g}$ transition.

The higher energy shoulders at 4.66 and 4.54 eV in $Mo(CO)_6$ and $W(CO)_6$ were respectively assigned to the $^1T_{2g}$ ($t_{2g}^5eg^1$) LF state.

In the absence of other theoretical investigations, the interpretation of the spectra of the heavier carbonyls still relies on the original assignment by Beach and Gray.[3] In view, however, of the reassignment of the spectrum of $Cr(CO)_6$ suggested by both CASPT2[2] and ΔSCF-DFT calculations,[1] as well as by the present TDDFT results, the original interpretation of the spectra of $Mo(CO)_6$ and $W(CO)_6$ appears to be quite questionable. For this reason we revisit the electronic spectra of these molecules using a TDDFT approach that employs the scalar relativistic

Table 6. Relativistic (ZORA) and Nonrelativistic BP/ALDA and LB94/ALDA Singlet Excitation Energies (eV) of $Mo(CO)_6$[a]

		transition energy (eV)					oscillator strength	
state	composition	BP/ZORA	LB94/ZORA	BP/n.r.	LB94/n.r.	expt[b]	BP/ZORA	expt[b]
a^1E_u	$100\%(2t_{2g}\rightarrow 9t_{1u})$	3.64	3.43	3.65	3.43			
a^1T_{2u}	$100\%(2t_{2g}\rightarrow 9t_{1u})$	3.67	3.45	3.67	3.45			
a^1A_{2u}	$98\%(2t_{2g}\rightarrow 9t_{1u})$	3.78	3.55	3.78	3.55			
a^1T_{1u}	$64\%(2t_{2g}\rightarrow 9t_{1u})$, $36\%(2t_{2g}\rightarrow 2t_{2u})$	3.88	3.60	3.88	3.59	4.33	0.04	0.15
a^1A_{1u}	$99\%(2t_{2g}\rightarrow 2t_{2u})$	4.19	3.82	4.19	3.81			
b^1T_{2u}	$100\%(2t_{2g}\rightarrow 2t_{2u})$	4.25	3.88	4.25	3.87			
b^1E_u	$100\%(2t_{2g}\rightarrow 2t_{2u})$	4.25	3.88	4.25	3.87			
a^1T_{1g}	$100\%(2t_{2g}\rightarrow 2t_{1g})$	5.13	4.63	5.12	4.60			
a^1T_{2g}	$100\%(2t_{2g}\rightarrow 2t_{1g})$	5.18	4.67	5.16	4.64			
b^1T_{1u}	$60\%(2t_{2g}\rightarrow 2t_{2u})$, $34\%(2t_{2g}\rightarrow 9t_{1u})$	5.73	5.40	5.68	5.34	5.45	2.16	2.20
a^1E_g	$66\%(2t_{2g}\rightarrow 2t_{1\,g})$, $23\%(2t_{2g}\rightarrow 3t_{2\,g})$	5.88	5.40	5.81	5.33			
b^1T_{1g}	$100\%(2t_{2g}\rightarrow 3t_{2g})$	5.91	5.46	5.78	5.34			
b^1T_{2g}	$92\%(2t_{2g}\rightarrow 3t_{2\,g})$	6.14	5.72	6.02	5.60			
b^1E_g	$70\%(2t_{2g}\rightarrow 3t_{2\,g})$, $20\%(2t_{2g}\rightarrow 2t_{1\,g})$	6.41	5.98	6.34	5.89			
c^1T_{2g}	$99\%(2t_{2g}\rightarrow 9a_{1g})$	6.49	7.44	6.50	7.49			
c^1T_{1g}	$100\%(2t_{2g}\rightarrow 6e_g)$	6.57	6.38	6.39	6.19			
d^1T_{2g}	$91\%(2t_{2g}\rightarrow 6e_g)$	6.77	6.59	6.60	6.40			
c^1A_{1g}	$75\%(2t_{2g}\rightarrow 3t_{2\,g})$, $12\%(5e_g\rightarrow 6e_g)$	8.30	7.92	8.18	7.80			

[a] Comparison is made to the experimental values. The one-electron transitions contributing to the TDDFT solution vectors and oscillator strengths are from relativistic BP/ALDA calculations. [b] From ref 3.

Table 7. Relativistic (ZORA) and Nonrelativistic BP/ALDA and LB94/ALDA Singlet Excitation Energies (eV) of $W(CO)_6$[a]

		transition energy (eV)					oscillator strength	
state	composition	BP/ZORA	LB94/ZORA	BP/n.r.	LB94/n.r.	expt[b]	BP/ZORA	expt[b]
a^1E_u	$99\%(2t_{2g}\rightarrow 9t_{1u})$	3.55	3.37	3.59	3.39			
a^1T_{2u}	$100\%(2t_{2g}\rightarrow 9t_{1u})$	3.58	3.40	3.62	3.41			
a^1A_{2u}	$99\%(2t_{2g}\rightarrow 9t_{1u})$	3.71	3.51	3.74	3.51			
a^1T_{1u}	$62\%(2t_{2g}\rightarrow 9t_{1u})$, $38\%(2t_{2g}\rightarrow 2t_{2u})$	3.80	3.55	3.84	3.56	4.30	0.04	0.18
a^1A_{1u}	$99\%(2t_{2g}\rightarrow 2t_{2u})$	4.13	3.79	4.15	3.79			
b^1E_u	$100\%(2t_{2g}\rightarrow 2t_{2u})$	4.20	3.85	4.21	3.85			
b^1T_{2u}	$100\%(2t_{2g}\rightarrow 2t_{2u})$	4.20	3.85	4.22	3.85			
a^1T_{1g}	$100\%(2t_{2g}\rightarrow 2t_{1g})$	5.11	4.62	5.06	4.55			
a^1T_{2g}	$100\%(2t_{2g}\rightarrow 2t_{1g})$	5.15	4.66	5.10	4.59			
b^1T_{1u}	$60\%(2t_{2g}\rightarrow 2t_{2u})$, $34\%(2t_{2g}\rightarrow 9t_{1u})$	5.84	5.52	5.70	5.36	5.53	2.41	3.30
a^1E_g	$82\%(2t_{2g}\rightarrow 2t_{1\,g})$, $6\%(2t_{2g}\rightarrow 3t_{2g})$	6.00	5.52	5.84	5.35			
b^1T_{1g}	$100\%(2t_{2g}\rightarrow 3t_{2g})$	6.47	5.93	6.02	5.51			
b^1T_{2g}	$93\%(2t_{2g}\rightarrow 9a_{1g})$	6.59	7.41	6.60	7.50			
c^1T_{2g}	$90\%(2t_{2g}\rightarrow 3t_{2\,g})$	6.71	6.19	6.25	5.77			
b^1E_g	$85\%(2t_{2g}\rightarrow 3t_{2\,g})$, $6\%(8t_{1u}\rightarrow 9t_{1u})$	6.86	6.37	6.48	6.01			
c^1T_{1g}	$100\%(2t_{2g}\rightarrow 6e_g)$	7.33	7.14	6.72	6.47			
d^1T_{2g}	$100\%(2t_{2g}\rightarrow 6e_g)$	7.44	7.26	6.88	6.64			
c^1A_{1g}	$63\%(2t_{2g}\rightarrow 3t_{2\,g})$, $16\%(7t_{1u}\rightarrow 9t_{1u})$	8.68	8.35	8.33	7.94			

[a] Comparison is made to the experimental values. The one-electron transitions contributing to the TDDFT solution vectors and the oscillator strengths refer to relativistic BP/ALDA calculations. [b] From ref 3.

ZORA orbitals and one-electron energies. Since spin−orbit coupling is neglected, the O_h single group symmetry classification is used as in the case of $Cr(CO)_6$.

The calculated spin-allowed excitation energies of $Mo(CO)_6$ and $W(CO)_6$ are presented in Tables 6 and 7, respectively, and compared to the available experimental information for the two allowed charge-transfer states. Since relativistic and nonrelativistic TDLDA calculations have been performed, using in both cases two different XC potentials, BP and LB94, four sets of results are gathered in Tables 6 and 7. Of course the excitation energies change in absolute value from one set of calculations to the other. We will discuss below the relativistic effects and the effect of the XC potential. Taking for the moment an overall view, we note that all four sets of results come to the same ordering of the excited states. In particular, they all agree on a crucial point for the interpretation of the spectra, which is that, just as in $Cr(CO)_6$, the lowest excited states have CT character and not the LF character suggested originally by Gray and Beach. In the singlet excited-state manifold, the lowest excited states are indeed the a^1E_u, a^1T_{2u}, a^1A_{2u} set of symmetry-forbidden CT states located below the first allowed $^1T_{1u}$ state and the a^1A_{1u}, b^1T_{2u}, b^1E_u, a^1T_{1g}, a^1T_{2g} set of symmetry-forbidden CT states located below the second allowed $^1T_{1u}$ state.

As shown in Tables 6 and 7, at the relativistic BP/ALDA level, the two spin-allowed and orbitally-allowed $^1A_{1g}\rightarrow{}^1T_{1u}$ transitions are calculated in $Mo(CO)_6$ at 3.88 and 5.73 eV, respectively, and in $W(CO)_6$ at 3.80 and 5.84 eV. The agreement with the experimental band maxima at 4.33 and 5.45 eV in $Mo(CO)_6$ and 4.30 and 5.53 eV in $W(CO)_6$ is satisfactory, particularly for the second band. LB94/ALDA results are in closer agreement with the experiment for the b^1T_{1u} state, but give the a^1T_{1u} at too low energy.

As found in $Cr(CO)_6$, the oscillator strengths of both $^1A_{1g}\rightarrow{}^1T_{1u}$ transitions are underestimated, although an exception is given by the oscillator strength of the $Mo(CO)_6$ b^1T_{1u} state which is calculated in very good agreement with experiment.

As inferred from the composition of the BP/ALDA solution vectors, the multiconfigurational character of the a^1T_{1u} and b^1T_{1u} excited states observed in $Cr(CO)_6$ still holds in the heavier carbonyls.

According to our calculations, the LF excited states are above these CT states and considerably higher than in $Cr(CO)_6$ as well.

From the composition of the relativistic BP/ALDA solution vectors reported in Tables 6 and 7, one can recognize the singlet ligand field states as the c^1T_{1g} and d^1T_{2g} states calculated at the relativistic BP/ALDA level at 6.57 and 6.77 eV in $Mo(CO)_6$ and at 7.33 and 7.44 eV in $W(CO)_6$. The LB94/ALDA energies are somewhat lower, but by no more than 0.2 eV. The corresponding triplet states are the c^3T_{1g} and c^3T_{2g} states calculated at the relativistic BP/ALDA level at 6.33 and 6.35 eV in $Mo(CO)_6$ and the c^3T_{1g} and e^3T_{2g} states calculated at the relativistic BP/ALDA level at 7.09 and 7.19 eV in $W(CO)_6$, respectively. Again the LB94 excitation energies are about 0.2 eV lower than the BP ones.

Besides the LF states, also the CT states arising from the $(2t_{2g})^5(3t_{2g})^1$ configuration are found to be much higher in the heavier carbonyls than in $Cr(CO)_6$, which is consistent with the upward shift in energy of both the 6eg and $3t_{2g}$ orbitals on going from Cr to Mo and W.

In view of these results, the original assignment by Beach and Gray[3] of the low-energy weak shoulders observed in $Mo(CO)_6$ and $W(CO)_6$ as LF transitions (the $^1A_{1g}\rightarrow{}^3T_{1g}$ transition and vibrational components of the $^1A_{1g}\rightarrow{}^1T_{1g}$ transition) and the higher energy weak shoulder between the strong CT bands as the $^1A_{1g}\rightarrow{}^1T_{2g}$ LF transition has to be revised. The TDLDA calculated LF transitions are roughly 3 eV above the lowest (orbital forbidden) CT transitions and 2−3 eV above the lowest allowed CT transition. It is unlikely that the TDLDA method would overestimate the LF transitions by that much, in particular since in $Cr(CO)_6$ the independent evidence coming from the CASPT2 calculations agrees reasonably well (LF excitations ca. 0.5 eV lower) with the TDLDA results.

Spin−orbit (SO) coupling may have some effect on the position of the excitation energies for $W(CO)_6$. We were unable to rigorously check this, as a TDDFT implementation which includes spin−orbit effects is not yet available. However, the magnitude of the spin−orbit effect is expected to be small. An order of magnitude estimate can be obtained from the orbital energies. If SO coupling is included in the SCF calculation, the $2t_{2g}$ level splits up by only 0.2 eV and the $6e_g$ level goes up. Therefore, SO effects will not decrease the LF splitting by more then a few tenths of an electronvolt. In view of the large difference, in the order of 3 eV, which we find between the CT and LF excitation energies at the scalar ZORA level, our conclusions will certainly not be affected by the full inclusion of SO effects.

On the basis of the results in Tables 6 and 7, the weak shoulders at the low-energy side of the first allowed band should be assigned as spin-allowed but symmetry-forbidden CT transitions of which there are plenty in the 3.5−4.0 eV region. We should maybe mention that there are in the same energy region also spin-forbidden but orbitally-allowed $^1A_{1g}\rightarrow a,b^3T_{1u}$ transitions. As for the high-energy shoulder, experimentally at 4.66 and 4.54 eV in $Mo(CO)_6$ and $W(CO)_6$, respectively, the calculated excitation energies at the LB94/ALDA level suggest the close-lying $^1A_{1g}\rightarrow a^1T_{1g}$ and $^1A_{1g}\rightarrow a^1T_{2g}$ symmetry-forbidden charge-transfer transitions to occur at this energy, with a clear separation from the nearest excitations.

Comparing BP/ALDA and LB94/ALDA results we notice that in the heavier carbonyls the effects of the choice of the XC functional on the excitation energies are very similar to those observed in $Cr(CO)_6$, the LB94 excitation energies being in general lower than the BP ones by 0.2−0.5 eV, irrespective of the type of calculation (singlet or triplet excitation energies, relativistic or nonrelativistic). Since high-quality ab initio calculations to which we could compare our results are not available, one cannot establish whether LB94 improves upon BP here (and for which states), although we have seen that in $Cr(CO)_6$ the LB94 results are closer to CASPT2 than the BP ones. Overall, the large differences between the BP/ALDA and LB94/ALDA excitation energies in all three members of the series demonstrate that even for quite "normal" excitations the effect of the choice of XC potential is very important. The sensitivity to the choice of potential of the excited states under consideration, which are diffuse but in most cases not at all Rydberg-like, indicates that not only the asymptotic behavior of the potential is an important factor here, but that the behavior in the region with important electron density has to be taken into account as well. This is underlined by the effects for the LF excited states, which show, as they did in $Cr(CO)_6$, an energy shift (about 0.2 eV) on going from BP to LB94. This occurs despite the nominally d−d character of these excitations.

As for the Rydberg excited states corresponding to the transition to the metal-$9a_{1g}$ orbital, they are just as in $Cr(CO)_6$ calculated at the LB94/ALDA level about 1 eV *higher* than at the BP/ALDA level.

We now turn to the relativistic effects on the excitation energies. It can be seen from Tables 6 and 7 that these effects are negligible for the states which involve transitions to the "pure" ligand orbitals, the $9t_{1u}$, the $2t_{1g}$, and the $2t_{2u}$, as could be expected. On the other hand, relativity increases by a sizable amount the energy of both the LF states and the CT states arising from the $(2t_{2g})^5(3t_{2g})^1$ configuration. This effect, which is much larger in $W(CO)_6$ (about 0.4 eV on average) than in $Mo(CO)_6$ (about 0.2 eV on average), is understandable in terms of the relativistic destabilization of the 4d and especially of the 5d orbitals and the resulting upward shift of the $6e_g$ and of the $3t_{2g}$ MOs that was discussed in section 3.

5. Concluding Remarks

Relativistic time dependent density functional calculations have been performed on the excited states of the $M(CO)_6$ (M = Cr, Mo, W) series. Our results indicate, in agreement with previous ΔSCF[1] and CASPT2[2] calculations on $Cr(CO)_6$, that in all members of the series the lowest excited states in the spectra do not correspond to ligand field excitations, as has been accepted in the past. Instead they correspond to CT states. According to our calculations, the bands appearing as shoulders at the low-energy side of the spectrum and between the two intense absorption bands have to be assigned to orbitally-forbidden or symmetry-forbidden charge-transfer states, which is consistent with the observed insensitivity of their position to the metal. The low intensity of these shoulders is to be attributed then to their forbidden nature, not to their LF character.

The LF excitations are calculated at much higher energy than suggested by the original assignment by Beach and Gray[3] and at different energy along the $M(CO)_6$ series, being much higher in the heavier carbonyls than in $Cr(CO)_6$.

These results lead to a reassessment of the role of the LF states in the photochemical dissociation of the meta−-CO bonds in the $M(CO)_6$ series. They strongly suggest indeed that the experimentally observed photodissociation of the M−CO bond upon irradiation into the lowest energy bands occurs in the heavier carbonyls, just as found in $Cr(CO)_6$, from CT and not from LF states. The photochemistry of the heavier carbonyls is currently being investigated and will be the subject of a forthcoming paper.

Comparison with the experimental data available and, in the case of $Cr(CO)_6$, with previous ΔSCF-DFT[1] and high-level correlated ab initio calculations,[2] allows for an assessment of

the reliability of the present TDDFT approach. The previously employed ΔSCF method proves to be fairly reliable when there is little configuration mixing, but is inadequate in cases of strong configuration mixing.

The choice of the XC functional is found to have a considerable effect on the excitation energies, the LB94 results for $Cr(CO)_6$ being usually closer to CASPT2[2] than the BP ones, demonstrating that even for quite "normal" excitations (not only high excitations, not only Rydberg transitions) the XC functional may play an important role. Neither the LB94/ALDA compared to BP/ALDA excitation energies nor the CASPT2 compared to LB94/ALDA excitation energies are universally in closer agreement with experiment.

In the heavier carbonyls, mostly in $W(CO)_6$, relativistic effects are seen to be relevant for the LF states as well as for the CT states arising from the $(2t_{2g})^5(3t_{2g})^1$ configuration. This effect is traced to the relativistic destabilization of the d orbitals and to the consequent upward shift of the $6e_g$ and of the $3t_{2g}$ MOs.

Acknowledgment. The authors wish to thank the Stichting Nationale Computer Faciliteiten (NCF) of The Netherlands Foundation for Scientific Research (NWO) for computing facilities.

Supporting Information Available: Tables 8 and 9, containing triplet excitation energies for $Mo(CO)_6$ and $W(CO)_6$, respectively (PDF). This material is available free of charge via the Internet at http://pubs.acs.org.

JA990747T